Crosshatch Surface Patterns—Comparison of Experiment with Theory

C. O. WHITE* AND R. M. GRABOW†
Aeronutronic Division of Philco-Ford Corporation, Newport Beach, Calif.

Experimental crosshatch patterns from ablating, melting, and flowing materials in supersonic flow are compared with theory. Results from wind-tunnel, rocket motor, and flight test environments on cones from 4.5° to 40° half-angles are shown to have common characteristics and to correlate in terms of relatively simple parameters. The theories considered include differential ablation, inelastic deformation, and liquid layer instability mechanisms. The experimental data are best correlated by a theoretical model which encompasses both the inelastic deformation and liquid layer mechanisms.

Nomenclature

$\bar{c}_i$ = imaginary part of complex wave velocity
$\bar{c}_r$ = real part of complex wave velocity
c_p = specific heat
G = shear modulus
h = static enthalpy
k = diffusivity parameter
K = thermal diffusivity
K^* = proportionality between internal shear and pressure perturbations
$\dot{m}$ = ablation rate
M = Mach number
$\tilde{M}$ = molecular weight
p = pressure
p' = pressure perturbation
$\hat{P}_{\text{mag}}$ = dimensionless pressure perturbation amplitude
q = heat-transfer rate
$\dot{s}$ = surface recession rate
t = time
T = temperature
u = velocity
x = distance normal to waves
$\bar{\alpha}$ = wave number, $2\pi/\lambda_N$
β = Mach angle
γ = ratio of specific heats
δ = boundary-layer thickness
δ_f = frictional sublayer thickness
δ_L = melt layer or viscoelastic layer thickness
ε = amplitude of surface wave
λ_L = streamwise wavelength
λ_N = wavelength normal to waves
μ = viscosity
Ω_p = pressure perturbation parameter
ρ = density
Λ = thermal conductivity
τ = shear stress
τ_R = material relaxation time
ϕ_p = pressure phase angle from maximum slope point
ϕ_τ = shear phase angle with respect to ϕ_p
ω = wave angle

Subscripts
e = edge of boundary layer
L = melt or viscoelastic layer
r = recovery
s = solid material
w = wall

Presented as Paper 72-313 at the AIAA 7th Thermophysics Conference, San Antonio, Texas, April 10–12, 1972; submitted May 18, 1972; revision received March 7, 1973. This work was supported by Air Force Space and Missile Systems Organization, Contract F04701-71-C-0014.

Index categories: Material Ablation; Boundary Layers and Convective Heat Transfer—Turbulent.

* Staff Member, Systems Engineering. Member AIAA.
† Section Supervisor, Aerothermodynamics. Member AIAA.

I. Introduction

CROSSHATCH surface patterns have been observed on a wide variety of dissimilar materials exposed to high-speed flow, including, among others, silicone fluid,[1] wax,[2] camphor,[3-6] ammonium chloride,[7,8] plastics,[3,9-13] Teflon,[7,14-16] Phenolics,[14] and graphite.[7] Practical interest originally centered on flight dynamic perturbations,[1] and heating increments[7] associated with pattern onset. More recently, it has been found that pattern-induced roughness heating also affects nosetip shape change,[6] and wave formations in both melting liquids and low-temperature ablator materials have been studied to obtain a better understanding of low-temperature simulation techniques for high-temperature phenomena.[17]

Crosshatch patterns are time-varying phenomena; they travel downstream and occasionally exhibit transients in wave angle and wavelength. In ground tests, there is often an initial quiescent phase, followed by abrupt crosshatch breakout over major portions of the model surface. With continued exposure, the patterns grow in depth. Ultimately, the organized criss-cross grid breaks down into a semirandom series of pits and gouges termed a regmaglypt[3] or scalloped surface. The Teflon cone of Fig. 1 (exposed to a gradient flowfield environment) illustrates all three stages of development. The afterbody is smooth, typical of a precrosshatched surface, the midsection shows orderly criss-cross grooves, while the forward portion exhibits the advanced development degenerate patterns of the scallop type. These processes can occur rapidly or slowly, depending on the test environment and model material. For low-viscosity liquid layers, the initial phases are not usually observed and the patterns immediately establish the terminal equilibrium configuration.

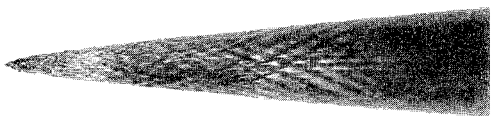

Fig. 1 Typical surface patterns on Teflon.

The present investigation is concerned with the initial stages of pattern development. The objective is to predict pattern onset and the resulting wavelength and wave angle. This is accomplished by correlating experimental data in terms of theoretically-derived parameters. The experimental data stem from wind-tunnel, arcjet, rocket motor and flight test environments, and encompass a variety of materials ranging from silicone fluid to graphite. In general, the data were obtained on cone and biconic configurations with half angles ranging from 4.5° to 40°.[1-5,7,12-14,18,19]

II. Theory

Most theoretical approaches for predicting surface patterns involve linear stability analyses. The objective is to determine the conditions which cause small disturbances to be amplified into visible surface patterns. The initial disturbances are generally assumed to result from a sinusoidal wavy surface of small amplitude (ε_0). The variation in amplitude is expressed in the generalized form

$$\varepsilon = \varepsilon_0 \exp\left[i\bar{\alpha}(x-\bar{c}t)\right] \tag{1}$$

Solutions to the stability equations for flow over the sinusoidal wall yield disturbance growth rates that can be positive (amplified) or negative (damped), depending on the assumed wavelength. Practical interest centers on solutions where combinations of amplifying and damping terms produce either zero or maximum amplification rates. The former condition establishes the neutral stability (pattern onset) criterion, while the latter condition defines the most probable or "preferred" pattern geometry. In general, the amplifying terms are found to arise from the perturbations in the gas boundary layer while the damping terms are related to the surface response mechanism. The three cross-hatching mechanisms that have been theoretically examined are: differential ablation, inelastic material deformation, and liquid layer instability. The following subsections describe briefly the principal features of each approach in order that the theories may be compared to each other and to experimental data.

Differential Ablation Theory

Differential ablation theory assumes the dominant amplifying effect to be the boundary-layer heat-transfer perturbation, which relates directly to the ablation rate perturbation for most ablating materials. Amplification results from high heating in the valleys and low heating on the crests of the wavy surface such that the differential ablation increases the amplitude of the surface waves. Inger[20] has obtained a closed-form solution to the governing stability equations

$$\bar{\alpha}\bar{c}_i = \frac{\dot{m}_w'}{\dot{m}_w}\frac{\dot{s}}{\varepsilon} = \frac{\dot{s}}{h_w}\frac{q_w}{\mu_w}\left\{2.34|\Omega_p|\sin(\phi_p-42) - \frac{c_{p_s}\mu_w h_s}{2\Lambda_s h_w}\left[(1+k^2)^{1/2}-1\right]\right\} \tag{2}$$

where

$$|\Omega_p| = \frac{\bar{\alpha}\delta_f{}^2 p'_{\text{mag}}}{\varepsilon\tau_{w_N}}, \quad \delta_f = \left(\frac{\mu_w{}^2}{\rho_w\tau_{w_N}\bar{\alpha}}\right)^{1/3}, \quad k = \frac{2\Lambda_s\bar{\alpha}}{c_{p_s}\dot{m}_w}$$

The first term in the brackets represents the amplifying effect of the boundary-layer heat-transfer perturbation which is shown to lag the pressure perturbation by 42°. The second term represents the damping effect of the surface heat conduction perturbation. The importance of this damping term is also evident in the differential ablation analyses of Lees and Kubota[21] and Lane and Ruger.[22] By introducing a pressure perturbation amplitude

$$\hat{P}_{\text{mag}} = \frac{p'_{\text{mag}}/p_e}{\gamma\varepsilon/\delta} \tag{3}$$

and performing several simplifications, the present authors[23] have derived the result

$$\bar{\alpha}\bar{c}_i = \frac{6.0}{\sin^2\omega}\frac{\dot{s}}{u_e}\frac{(h_r-h_w)}{h_w}p_e\left(\frac{\mu_w{}^{1/2}}{\rho_w\tau_w\lambda_L{}^2}\right)^{2/3}\left[\frac{\hat{P}_{\text{mag}}\sin(\phi_p-42)}{\delta/\lambda_L}\right] - \frac{39.5}{\sin^2\omega}\frac{\dot{s}}{\delta}\frac{h_s}{h_w}\frac{K}{\dot{s}\delta}\left(\frac{\delta}{\lambda_L}\right)^2 \tag{4}$$

The quantity, $\hat{P}_{\text{mag}}\sin(\phi_p-42)/(\delta/\lambda_L)$ may be obtained from existing solutions of the perturbed boundary layer flow.[20,21,24]‡ These solutions are all based on inviscid flow analyses, and in some cases involve two-dimensional flow assumptions. The present investigation utilizes the three-dimensional inviscid solutions of Donaldson and Conrad.[24] It is found that the amplification rates attain a maximum value when plotted vs wave angle (ω) for a given value of the wavelength ratio (δ/λ_L). This maximum value defines the preferred wave angle (i.e., the pattern angle) corresponding to a particular wavelength.

For neutral stability ($\bar{\alpha}\bar{c}_i = 0$),

$$\left(\frac{\delta}{\lambda_L}\right)_{\alpha c_i=0} = \frac{0.06}{(K/\dot{s}\delta)^{1.5}}\left(\frac{h_r-h_w}{h_s}\right)^{1.5}\left(\frac{p_e}{u_e}\right)^{1.5}\frac{\mu_w{}^{0.5}}{\rho_w\tau_w\delta^{0.5}}\times\left[\frac{P_{\text{mag}}\sin(\phi_p-42^\circ)}{\delta/\lambda_L}\right]^{3/2} \tag{5}$$

Inelastic Deformation Theory

Inelastic deformation theory assumes the dominant amplifying effect to result from the internal shear perturbations in a soft viscoelastic material. Analyses by Probstein and Gold[18] assume the internal shear proportional to the boundary-layer shear which is related to the boundary-layer pressure perturbation signature. Surface responses have been evaluated for Kelvin and Maxwell deformation models. Since the latter is more applicable to flight materials of interest, only solutions based on the Maxwell model are considered here. The closed-form amplification rate solution for this case is

$$\bar{\alpha}\bar{c}_i = (K^*u_e/\bar{\alpha}\delta^2\tau_R)\hat{P}_{\text{mag}}\sin(\phi_p+\pi/2+\phi_\tau) \tag{6}$$

where

$$\tau_R = (\mu_L/G)(u_e/\delta) \quad \text{and} \quad K^* \sim \tau_w/G\sin\omega$$

The phase lag angle (ϕ_τ) between the pressure and shear perturbations was assumed by Probstein and Gold to be $-120°$. Inger[20] has shown that this result is correct for adiabatic surfaces, but for high heat-transfer cases, the phase lag angle approaches $-60°$.

Since Eq. (6) contains no damping terms, it always predicts positive amplification for pressure phase angles, $\phi_p > 30°$. The lack of a damping term is rooted in the basic response model which assumes a uniform viscoelastic surface of infinite depth. For this reason Eq. (6) is unable to predict a neutral stability or maximum amplification condition. However, it is capable of showing the relationship between wave angle and wavelength. This is demonstrated by substituting for τ_R, K^*, and ϕ_τ in Eq. (6) to yield

$$\bar{\alpha}\bar{c}_i \sim \frac{\tau_w}{\mu_L}\frac{\hat{P}_{\text{mag}}}{\delta/\lambda_L}\sin(\phi_p\pm 30) \tag{7}$$

where the positive sign is used for high heating conditions and the negative sign for low heating conditions. Plotting $\bar{\alpha}\bar{c}_i$ as a function of wave angle (ω), yields a well-defined maximum value for a specified wavelength ratio (δ/λ_L).

Since their amplification rate solution could not yield a pattern wavelength, Probstein and Gold have utilized the closed-form pattern wave speed solution for this purpose,

$$\bar{\alpha}\bar{c}_r = \frac{K^*u_e}{\bar{\alpha}\delta^2\tau_R}\hat{P}_{\text{mag}}\cos\left(\phi_p+\frac{\pi}{2}+\phi_\tau\right) \sim \frac{\tau_w}{\mu_L}\frac{\hat{P}_{\text{mag}}}{\delta/\lambda_L}\cos(\phi_p\pm 30) \tag{8}$$

‡ In this study the pressure phase angle ϕ_p is measured upstream from the maximum slope point of the waves in accordance with Ingers notation. However, in the original reference other phase angle definitions were employed.

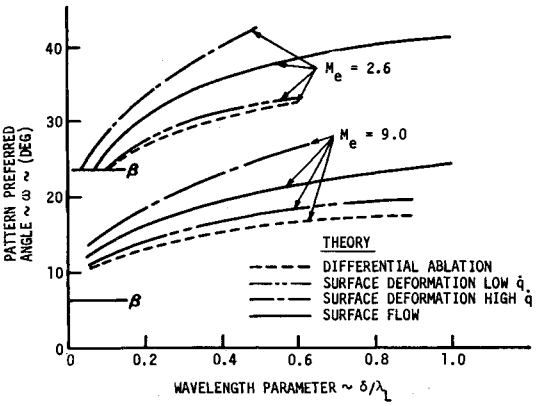

Fig. 2 Predicted wave angles—theory.

Since $\bar{\alpha}\bar{c}_r \sim u_e/\lambda_L$ by definition, and assuming that $\hat{P}_{mag}\cos(\phi_p \pm 30)/(\delta/\lambda_L)$ is independent of δ/λ_L, one obtains

$$\lambda_L \sim \mu_L u_e/\tau_w \tag{9}$$

This result provides a simple means of correlating experimental wavelength data, and will be discussed subsequently.

Surface Flow Theory

Surface flow theory is based on the instability that occurs when a slow flowing viscous layer interacts with a supersonic gas flow. The application of this type of mechanism to surface cross-hatching was first performed by Nachtsheim[25] who considered the case of a thin liquid layer interacting with a supersonic inviscid flow. While Nachtsheim used a uniform gas flow model, Grabow and White[23,27] analyzed the effect of a nonuniform boundary-layer gas flow. The latter analysis revealed that the dominant amplifying effect was the external pressure perturbation, while the dominant damping effect was the boundary-layer shear perturbation acting on the crests of the waves. The effects of surface tension and body forces were found to be negligible for all cases of interest. These results also indicated that a thin liquid layer analysis could also be applicable to thin viscoelastic layers, so that surface melting and deforming problems could be treated with the same analytical solution. It has recently been demonstrated by Lane[26] that this procedure is valid for large values of the spring constant in the Maxwell deformation model.

The amplification rate predicted by the Grabow-White generalized surface flow approach is

$$\bar{\alpha}\bar{c}_i = 18.4\left(\frac{\delta_L}{\lambda_L}\right)^3 \frac{p_e}{\mu_L}\frac{\hat{P}_{mag}}{\delta/\lambda_L}\sin\phi_p\left[1. - \frac{1.1\mu_w^{2/3}\lambda_L^{1/3}}{\delta_L(\rho_w\tau_w)^{1/3}}\right] \tag{10}$$

Plotting this equation as a function of wave angle yields a well-defined maximum amplification rate for a specified wavelength ratio (δ/λ_L). The resulting wave angle predictions are identical to those computed by Donaldson and Conrad[24] since their methodology was used to evaluate the pressure perturbation quantity $\hat{P}_{mag}\sin\phi_p/(\delta/\lambda_L)$. However, the angles are substantially different from those predicted by Nachtsheim's theory which are always equal to or slightly greater than the Mach angle; this is a direct consequence of the uniform gas flow assumption in Nachtsheim's theory.

In Ref. 27 a simplification to Eq. (10) was made assuming that the wavelength normal to the waves, λ_N, is directly proportional to δ_L (based on Nachtsheim's results). The functional form of the wavelength for neutral stability was then determined to be

$$\lambda_{N_0} \sim T_w^{1.1}/(P_e\tau_w)^{1/2} \tag{11}$$

Although the details are not provided, this result is readily derived from Eq. (10) by utilizing a perfect gas law and a viscosity temperature law.

The preceding discussion shows elements of similarity between the respective theories, yet there are differences which can serve to distinguish the operative physical mechanism. For example, all theories show a trend of increasing wave angle with the parameter δ/λ_L, but the magnitudes of the predicted wave angles are different. This result stems from the fact that the dominant amplifying term for each mechanism is proportional to the pressure perturbation quantity, $\hat{P}_{mag}\sin(\phi_p - \Delta\phi)/(\delta/\lambda_L)$, where $\Delta\phi$ is 42° for differential ablation theory, +30° for inelastic deformation theory with low heating (−30° for high heating), and zero for surface flow theory. Figure 2 illustrates typical wave angle predictions for the various theories at two Mach numbers. The observed variations are caused solely by the differences in $\Delta\phi$. Therefore, a comparison of experimental data with these results provides an indication of the dominant cross-hatching mechanism. It is noted that the pressure perturbation quantity, $\hat{P}_{mag}\sin(\phi_p - \Delta\phi)/(\delta/\lambda_L)$ is a function only of edge Mach number at the preferred wave angle condition.[23,24]

III. Correlations

Experimental Data

In subsequent plots, the data symbols representing body geometry often comprise averages of up to five of six individual readings at a given station. This procedure is required on conical surfaces because a relatively small percentage of the experimental grooves reflect the "preferred" geometry. The remaining grid elements are locally perturbed due to insertion of new grooves and other distortions accompanying the mapping of an intrinsically planar grid pattern onto an expanding conical surface.[7] To ensure consistency, all local flowfields have been evaluated using a common computer code which accounts for nose bluntness and mass addition effects. Flight vehicle local flowfields were evaluated for conditions near peak pressure, where the amplification rates are a maximum. Descriptions of tests, data processing, and results from more than 115 distinct test conditions involving 20 materials are provided in Ref. 7. Each symbol represents a separate model-flowfield combination, and multiple datum points under a common symbol represent successive body stations on the same model.

Pattern Wave Angle

Previous attempts to correlate pattern wave angles have concentrated on Mach number dependence.[13,14] However, all applicable theories show that wave angle is also a function of

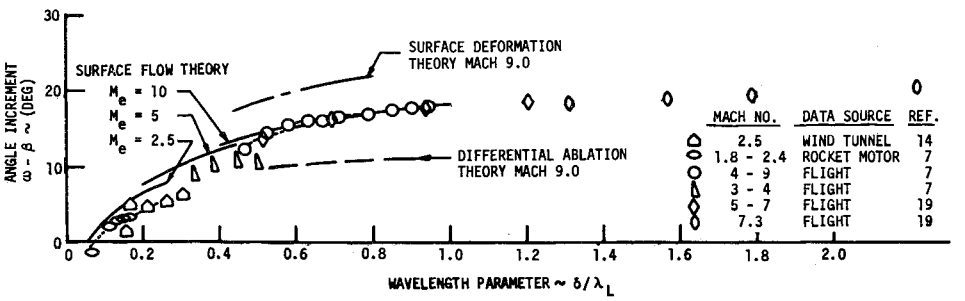

Fig. 3 Wave angle correlation—Teflon.

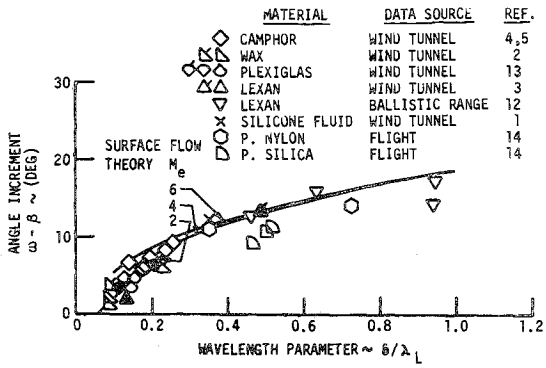

Fig. 4 Wave angle correlation—various materials.

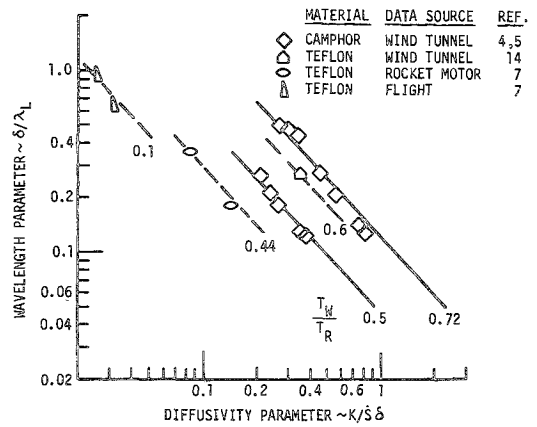

Fig. 5 Wavelength correlation—differential ablation theory.

the boundary-layer wavelength ratio δ/λ_L, such that various wave angles can occur at a common edge Mach number. Because the experimental data cover a wide range of Mach numbers, it is inconvenient to compare wave angles directly; however, it is observed from Fig. 2 that the angle increment $(\omega-\beta)$ as a function of δ/λ_L is relatively insensitive to edge Mach number for all theories. Figure 3 summarizes Teflon measurements from various ground and flight test data sources compared in this incremental format. There is striking consistency in the experimental data trends, particularly when it is considered that the patterns on flight vehicles were obtained under very high ablation rate conditions, those on the rocket motor exhaust model at moderate ablation rates, those on wind-tunnel models at little[14] or no ablation.[18] Furthermore, while most configurations were sharp cones with uniform flowfields, the rocket motor model and the blunt nosed flight vehicles had significant flowfield gradients. In spite of major variations in physical wave angle magnitudes, it is apparent from Fig. 3 that there is excellent agreement between ground and flight test experiments, and that all wave angle trends match very closely the predictions of surface flow theory. Differential ablation theory tends to predict wave angles that are too low, while surface deformation theory for high heating conditions predicts wave angles too high to match the flight data.

Figure 4 summarizes similar wave angle comparisons for a variety of materials. Included are results from melting, but not ablating, wax models,[2] melting and ablating plexiglas models,[13] Lexan models in a wind tunnel,[3] Lexan models in a ballistic range,[9] and data from recovered flight vehicles with phenolic nylon and refrasil heatshields. Also plotted is the single wave angle measurement from the liquid flow experiment of Nachtsheim,[1] wherein silicone fluid is released onto the surface of a cone from a slot near the nose. On a dimensional basis the experimental data illustrated in Fig. 4 span two orders of magnitude in streamwise wavelength, from $\lambda_L = 0.007$ in. to $\lambda_L = 0.87$ in., while wave angles cover a range of almost 30°. But in this normalized format, the data from all sources fall into a relatively narrow corridor similar in magnitude and consistent in trend with the previously discussed Teflon data and with the surface flow theory predictions.

One implication from Figs. 3 and 4 is that pattern wave angle is insensitive to material property. This is consistent with surface flow theory which predicts that the preferred pattern wave angle for maximum amplification is primarily a function of the external flow pressure perturbation field. Given a wavelength, there is a particular corresponding preferred pattern wave angle. This characteristic is further illustrated by the solid symbol datum points in Fig. 4. The triangle symbols represent early fine grain transient patterns and subsequent coarse grain (longer wavelength) patterns on the same Lexan model.[3] The other solid symbols represent identical configuration plexiglas models[13] at different tunnel total temperatures. In both cases, the changing wavelength is accompanied by a variation in wave angle such that the respective datum points follow the theoretical curve trend.

Pattern Wavelength

Unlike wave angle, wavelength predictions from respective theories cannot be compared directly. This is because the functional relationships and basic correlation parameters differ between the respective theories. To a certain degree this is expected since wave angle is determined largely by imposed external flow considerations (common to all theories and shown to be a function of the parameter δ/λ_L), while wavelength is sensitive to material response characteristics and hence is a function of material properties.

It was shown in Sec. II that differential ablation theory predicts a functional dependence for the wavelength ratio. For a given flowfield environment, Eq. (3) yields

$$\frac{\delta}{\lambda_L} \sim \left(\frac{1-T_w/T_r}{K/\dot{s}\delta}\right)^{1.5} \tag{12}$$

A preliminary correlation of camphor wavelength data in terms of these quantities is shown in Fig. 5. The influence of the diffusivity parameter $(K/\dot{s}\delta)$ is predicted reasonably well by the theory, but the observed heat-transfer effect is opposite to the theoretical trend. This discrepancy between experiment and theory on the role of heat transfer occurs for both the camphor and Teflon data. Since differential ablation theory also did not provide a good prediction of the pattern wave angle, it was subsequently abandoned by the present authors.

The wavelength functional dependence according to inelastic deformation theory [Eq. (9)] suggests that if viscosity for a particular material can be assumed constant, wavelength should be proportional to the ratio u_e/τ_w. Figure 6 illustrates that when models are in steady-state ablation (camphor datum points) wavelength is, indeed, a single valued function, but if melt flow or transient response is involved (wax, plexiglas, and low

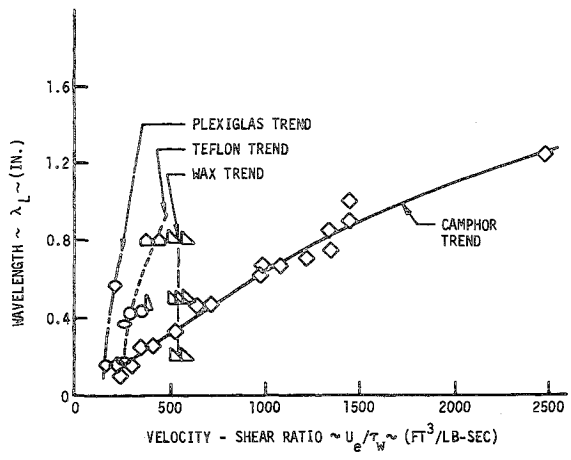

Fig. 6 Wavelength correlation—inelastic deformation theory.

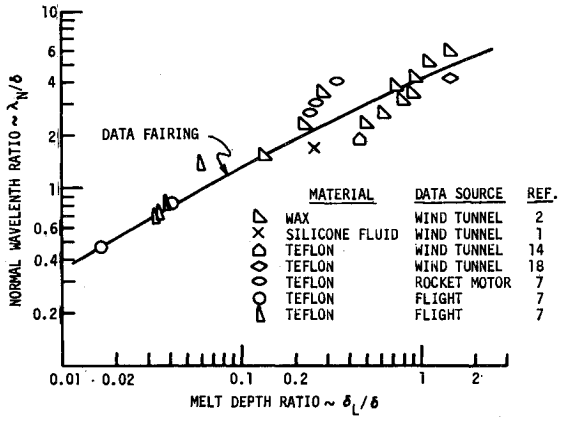

Fig. 7 Wavelength correlation as function of liquid layer depth.

ablation rate Teflon), the proportionality $\lambda_L \sim u_e/\tau_w$ is not maintained. This lack of correlation is attributed to the absence in the theory of a finite viscoelastic depth. By analogy with liquid layer phenomena, it is believed that the stability characteristics of a viscoelastic layer provides the necessary damping mechanism to sort out a preferred wavelength. To account for this effect, the present authors developed a general surface flow approach that is discussed briefly in Sec. II. The neutral stability solution [Eq. (11)] is based on an assumed normal wavelength proportionality, $\lambda_N \sim \delta_L$. However, the method is based on thin liquid layer assumptions and cannot predict thick liquid layer asymptotic behavior. Limited results from the Lane-Ruger theory[26] suggest that for thick liquid layers, wavelength becomes insensitive to liquid depth. Since experimental data fall between these two limits, we shall simply plot λ_N/δ as a function of δ_L/δ and let the resulting slope suggest the best wavelength-liquid depth functional dependence. Figure 7 shows that with this approach, experimental data from liquid silicone, melting wax, melting Teflon, moderate ablation rate Teflon, and high ablation rate Teflon (flight test), are fairly well correlated.

The calculated liquid layer depth used in Fig. 7 was obtained from a transient thermal response analysis.[7] Melt layer depth is defined in terms of a melt temperature or viscosity increment relative to the surface values. For Teflon a melt temperature of 900°R was utilized together with a melt vicosity of 10^4 poise. The wax melt temperature was taken as 606°R. An important result of these calculations was the demonstration of basic trend differences between melting and ablating models. The melting wax models show increasing liquid layer depth with increasing wind-tunnel total temperatures. This is because the tunnel recovery temperatures are only slightly greater than the melt temperatures; hence, increasing total temperature increases the thermal penetration rate and thermal thickness (for fixed exposure times). For rapidly ablating Teflon models, liquid layer depth decreases with increasing total temperature because surface recession rates increase faster than thermal penetration rates, thereby limiting the thickness of the thermally affected zone.

It is important to note that the surface flow mechanism does not require physical melt layer runoff; a slow creep is sufficient. The Teflon experimental data correlated in Fig. 7 have typical calculated surface flow rates in the range of 3×10^{-3} in./sec to 7×10^{-3} in./sec. Clearly, in the few seconds representative of typical test exposures, the material will not appear to move at all. Also, the viscosity-temperature curves of Ref. 7 show that many materials do not have a discrete "melt point" accompanied by a discontinuous change in viscosity, rather only a trend of continuously decreasing viscosity with increasing temperature. Nevertheless, it is readily visualized that such materials can develop a "deformation layer" wherein the viscosity at the surface is lower than in the substrata. This suggests that the terms "deformation layer" and "liquid layer" are synonymous in the general context of a surface flow with increasing subsurface viscosity determined by a temperature gradient.

The depth of the liquid or deformable layer for materials in a steady-state high ablation mode can be written as

$$\delta_L = (K/\dot{s}) \ln [(T_w - T_i)/(T_m - T_i)] \tag{13}$$

where T_w is the surface temperature, T_i the internal temperature, and T_m is the melt temperature, or for nonmelting materials, a reference temperature indicating an upper viscosity limit. This relation suggests that for large ablation rates, liquid layer depth is inversely proportional to surface recession rate. To demonstrate this feature, Fig. 8 shows a correlation of Teflon and camphor normalized wavelengths plotted as a function of inverse surface recession rate. For cases where the layer depth δ_L cannot easily be determined, but steady-state ablation does exist, Eq. (13) can be used to obtain a wavelength prediction. Assuming that $\lambda_L \sim \delta_L$ and applying Reynold's analogy to Eqs. (11) and (13) yields the following result for a given material with a specified surface temperature and melt temperature:

$$\lambda_L \sim 1/\dot{s} \sim 1/\tau_w \sim 1/p_e^{0.8} \tag{14}$$

This suggests that for equilibrium steady-state ablation, wavelength can be plotted as a function of surface pressure. Figure 9 shows that this is, indeed, the case for a wide range of materials under diverse flow conditions. Furthermore, the experimental slope ($\lambda_L \sim p_e^{-0.77}$) is close to the theoretically derived expression shown above. This trend of decreasing wavelength with increasing pressure has been observed previously by the present authors and others,[4] but it is now apparent that a correlation can only be obtained when deformation depth is inversely proportional to surface recession rate; hence, it cannot apply to melting models under transient thermal response conditions. Reference 23 discusses instances of measured wavelengths on melting wax and Teflon models which fail to conform to the pressure correlation.

The important results from the above are that under high ablation rate conditions, wavelengths can be determined directly from the pressure correlations of Fig. 9, and such wavelengths are indirect indices to the deformation depth. The appropriate (and possibly unknown) materials properties affecting layer depth appear as displacement shifts between the respective curves.

Pattern Onset and Growth

On the basis of the successful wave angle and wavelength correlations obtained with surface flow theory, the method was also used to correlate pattern onset conditions. There is an uncertainty concerning the appropriate wavelength-layer depth relationship. The correlations of Fig. 9 are not directly applicable because as shown by the numerical calculations of Nachtsheim[25] the wave number ratios $\alpha = 2\pi\delta/\lambda_N$ at peak amplification (typical of well-developed experimental patterns) are not directly proportional to the corresponding wave numbers at neutral stability. It is assumed, consistent with Nachtsheim's results, that at neutral stability the wavelength normal to the wave crests is proportional to the surface flow thickness (e.g., $\lambda_{N_0} \sim \delta_L$)

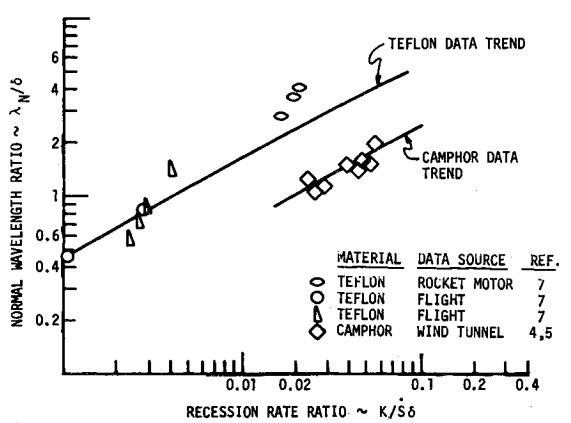

Fig. 8 Wavelength as function of recession rate.

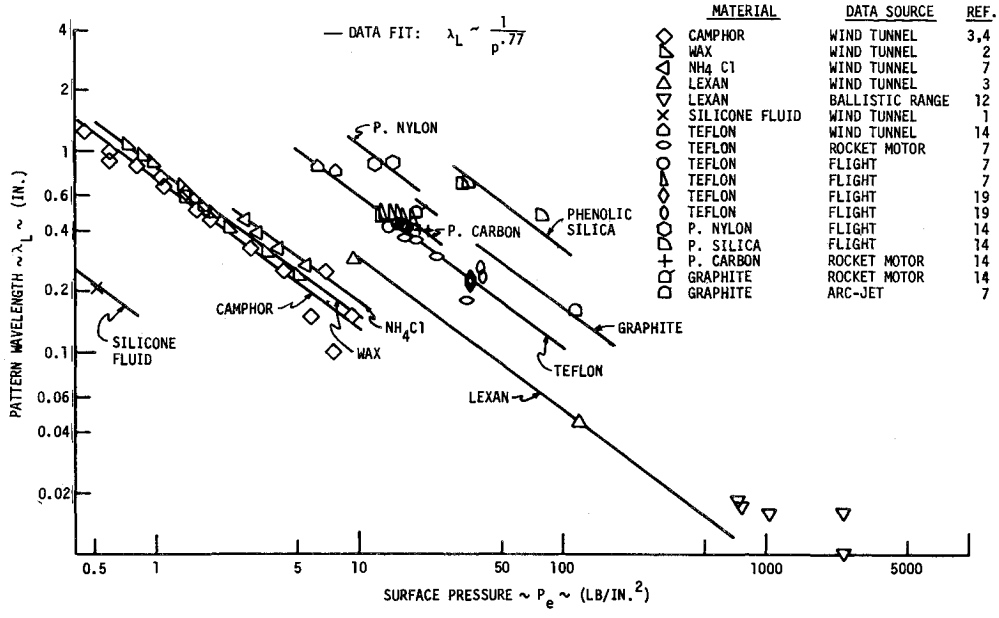

Fig. 9 Wavelength as function of pressure.

so that the normal wavelength for neutral stability is $\lambda_{N_0} \sim T_w^{1.1}/(p_e \tau_{w_N})^{1/2}$.

A correlation in terms of this parameter is presented in Fig. 10 for camphor and wax data. It is shown that all the crosshatched data lie well in the amplified region. The no-crosshatched data in the damped region represent calculated values of normal wavelength using the streamwise wavelength and wave angle correlations provided in Figs. 3 and 9. These are, therefore, the normal wavelengths that would exist if patterns did occur. A threshold level of $\simeq 24$ for the surface flow parameter is suggested by the data, although this result is not predicted. The theory predicts only a neutral stability boundary that has a slope of -1 when plotted in the format of Fig. 10. The data indicates that a smaller negative slope coupled with a threshold level would be more appropriate. It is noted that one of the simplifications leading to Eq. (11) involved an assumed proportionality between wavelength and viscoelastic or melt layer thickness. If one assumed a more appropriate relationship, it appears that the slope could be predicted more accurately. The threshold level is believed to be a function of the material response characteristics under transient heating conditions.

As previously mentioned, the present correlations are primarily applicable to materials experiencing steady-state ablation. The predicted pattern onset criterion for a range of high temperature ablation materials is presented in Fig. 11. The results clearly show the fully crosshatched data to be inside the amplified region, the incipient crosshatched data to be close to the stability boundary, while the noncrosshatched data lie within the damped region. In addition, the predicted slope of -1 is confirmed by the experimental data.

The recovered flight vehicles include configurations both with and without patterns on both Teflon and Phenolic Silica materials. The correlation onset boundary correctly distinguishes the respective behavior trends.

The pattern onset correlations (Figs. 10 and 11) may be easily used to predict if patterns will occur in ground or flight test environments. From computations of surface pressure, shear, temperature, Mach number, and boundary-layer thickness, one can rapidly estimate if the normal wavelength (i.e., surrogate for deformation depth) is sufficiently large for an amplification condition to exist. The pattern geometry (streamwise wavelength and wave angle) at this condition are obtained from the correlations provided in Figs. 3 and 9. The pattern growth history is obtained from Eq. (1), expressed in the form,

$$\varepsilon = \varepsilon_0 \exp \int_0^t \bar{\alpha}\bar{c}_i \, dt \tag{15}$$

This exponential variation causes the pattern depth to be extremely sensitive to the net amplification rate, $\bar{\alpha}\bar{c}_i$. As discussed

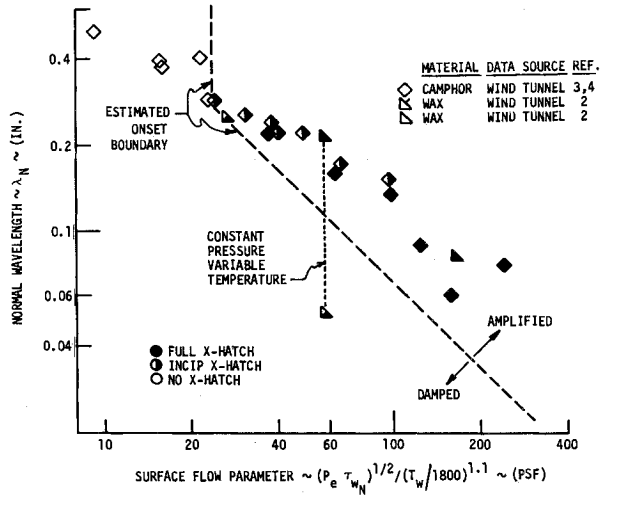

Fig. 10 Pattern onset correlation—low-temperature materials.

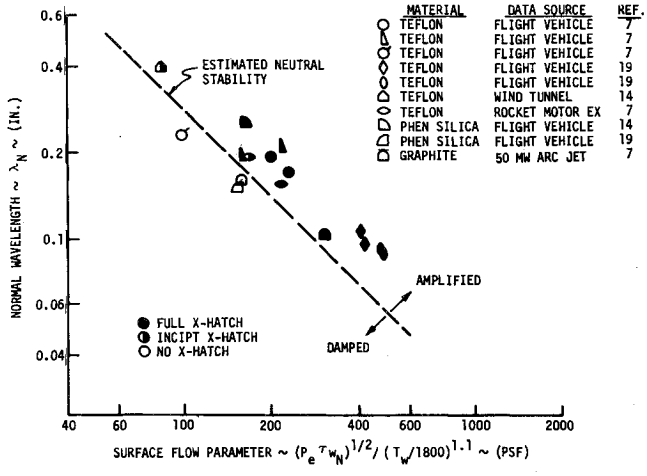

Fig. 11 Pattern onset correlation—high-temperature materials.

in Sec. II, the net amplification by surface flow theory is the difference between a pressure perturbation amplifying term and a shear perturbation damping term. However, examination of Eq. (9) reveals that the magnitude of the amplification rate for an unstable (amplified) condition is primarily influenced by the function

$$\bar{\alpha}\bar{c}_i \sim P_e/\mu_L \tag{16}$$

This result qualitatively explains the experimental evidence[7] that patterns are deeper in softer materials (low viscosity), and the depth distribution tends to correlate with the surface pressure distribution. However, it must be recognized that this functional dependence is based on a linear analysis, and is therefore applicable only in the early stages of pattern development. Some of the experimental data having deep patterns bears evidence of nonlinear effects.

IV. Conclusions

Experimental pattern data from ground and flight test environments on liquid film, melting, and ablating materials show similar behavior trends. The data are best correlated with parameters obtained from surface flow theory. Typical trends are as follows.

1) Pattern wave angle varies inversely with local Mach number and directly with the ratio of boundary-layer thickness to streamwise wavelength δ/λ_L.

2) Wavelength is primarily a function of melt layer or viscoelastic layer depth. Under equilibrium high ablation rate conditions where melt layer depth can be linked to surface recession rate, it is shown that wavelength decreases with pressure according to the relationship, $\lambda_L \sim p_e^{-0.77}$

3) Pattern onset conditions are correlated by the neutral stability parameters derived from surface flow theory. Instability is promoted by increases in pressure and shear, and decreases in surface temperature.

4) Pattern initial growth rate is an exponential function of the time-integrated net amplification rate. The dominant amplification term is primarily the ratio of surface pressure to material viscosity.

With the aid of these generalized trends, some previously unexplained features of experimental data are readily clarified. 1) Pattern wave angles on flight vehicles are typically larger than on ground test models at similar edge Mach numbers because of thicker boundary layers. 2) Increasing wave angles as a function of body station on ground test models, and invariance on conical flight vehicles, can be explained by the general variation of the ω vs δ/λ_L correlation curve. 3) Pattern wavelength is insensitive to body station on conical bodies having uniform surface pressure and high ablation rates. 4) Transient phenomena characterized by initial fine grain patterns replaced by coarse grain patterns are a natural result of varying melt layer or viscoelastic layer depth with exposure time. 5) Decreasing pressure promotes longer wavelengths but decreases net amplification rate. This may explain why streamwise wavelengths longer than one inch are almost never observed experimentally. Although instability may be present, the time of development is too long for visible patterns to appear within typical test durations.

Although surface flow theory provides the most satisfactory data correlations, it is possible that under certain specialized conditions (low Mach number, highly viscous material) the differential ablation mechanism can produce amplification rates of the same order as surface flow theory. The possibility that the patterns stem from both mechanisms operating in concert has not been investigated and merits further consideration.

References

[1] Nachtsheim, P. R. and Hagen, J. R., "Observations of Cross-hatched Wave Patterns in Liquid Films," *AIAA Journal*, Vol. 10, No. 12, Dec. 1972, pp. 1637–1640.

[2] Stock, H. and Ginoux, J. J., "Experimental Crosshatched Ablation Patterns," *AIAA Journal*, Vol. 9, No. 5, May, 1971, pp. 971–973.

[3] Larson, H. K. and Mateer, G. G., "Cross-Hatching—A Coupling of Gas Dynamics with the Ablation Process," AIAA Paper 68-670, Los Angeles, Calif., 1968.

[4] Williams, E. P., "Experimental Studies of Ablation Surface Patterns and Resulting Roll Torques," *AIAA Journal*, Vol. 9, No. 7, July, 1971, pp. 1315–1321.

[5] Williams, E. P. and Inger, G. R., "Investigations of Ablation Surface Cross-hatching," SAMSO TN-70-246, June 1970, U.S. Air Force.

[6] Baker, R. L. and Crowell, P. G., "Low Temperature Ablator Nose Tip Shape Change at Angle of Attack," AIAA Paper 72-90, San Diego, Calif., 1972.

[7] White, C. O., Grabow, R. M., and Moody, H. L., "Final Report, Small Vehicle Dynamics Study II, Cross-hatch Studies: Volume I—Data Survey and Data Processing," RSO Publication U-4972, Oct. 1971, Philco-Ford Corp., Newport Beach, Calif.

[8] McDevitt, J. B., "An Exploratory Study of the Roll Behavior of Ablating Cones," *Journal of Spacecraft and Rockets*, Vol. 8, No. 2, Feb. 1971, pp. 161–169.

[9] Wilkins, M. E., "Evidence of Surface Waves and Spreading Turbulence on Ablating Models," *AIAA Journal*, Vol. 3, No. 10, Oct. 1968, pp. 1963–1964.

[10] Wilkins, M. E. and Tauber, M. E., "Boundary Layer Transition on Ablating Cones at Speeds up to 7 km/sec," *AIAA Journal*, Vol. 4, No. 8, Aug. 1966, pp. 1344–1348.

[11] Canning, T. N., Wilkins, M. E., and Tauber, M. E., "Ablation Patterns on Cones having Laminar and Turbulent Flows," *AIAA Journal*, Vol. 6, No. 1, Jan. 1968, pp. 174–175.

[12] Canning, T. N., Tauber, M. E., and Wilkins, M. E., "Review of Recent Ballistic Range Boundary Layer Transition Work on Ablating Bodies at Ames," *Boundary Layer Transition Study Group Meeting*, Aerospace TR-0158 (538-16-63)-1, Vol. 3, Sec. 16, Aug. 1967, Aerospace Corp., San Bernardino, Calif.

[13] Canning, T., Tauber, M., Wilkins, M., and Chapman, C., "Orderly Three-Dimensional Processes in Turbulent Boundary Layers on Ablating Bodies," *Hypersonic Boundary Layers and Flow Fields*, AGARD conference proceedings CP 30, Sec. 6, May 1968.

[14] Laganelli, A. L. and Nestler, D., "Surface Ablation Patterns: A Phenomenology Study," *AIAA Journal*, Vol. 7, No. 7, July 1969, pp. 1319–1325.

[15] Laganelli, A. L. and Zemple, R. E., "Observations of Surface Ablation Patterns in Subliming Materials," *AIAA Journal*, Vol. 8, No. 9, Sept. 1970, pp. 1709–1711.

[16] Nachtsheim, P. R. and Larson, H. K., "Cross-Hatched Ablation Patterns in Teflon," *AIAA Journal*, Vol. 9, No. 8, Aug. 1971, pp. 1608–1614.

[17] Chen, C. J. and Ostrach, S., "Low Temperature Simulation of Hypersonic Melting Ablation and Observed Wave Patterns," *AIAA Journal*, Vol. 9, No. 6, June 1971, pp. 1120–1125.

[18] Gold, H., Probstein, R. F., and Scullen, R., "Inelastic Deformation and Cross-Hatching," *AIAA Journal*, Vol. 9, No. 10, Oct. 1971, pp. 1904–1910.

[19] Roth, H., "SPARTA REVEP Technical Interchange Meeting," M-280, Feb. 1969, Chrysler Corp., Missile Div., Detroit, Mich.

[20] Inger, G. R., "Compressible Boundary Layer Flow Past a Swept Wavy Wall with Heat Transfer and Ablation," VKI TN 67, Dec. 1970, von Kármán Inst., Belgium.

[21] Lees, L. and Kubota, T., "Research on Fluid Mechanics of Striating Ablation," GALCIT Progress Rept. 1, 2, and 3, 1969, California Inst. of Technology, Pasadena, Calif.

[22] Lane, F. and Ruger, C., "Minutes of Technical Interchange and Technical Direction Meeting, Contract F04701-70-C-0163," May 5, 1971, General Applied Science Labs., Westbury, N.Y.

[23] White, C. O. and Grabow, R. M., "Final Report, Small Vehicle Dynamics Study II, Cross-hatch Studies, Volume II—Theory, Correlations, and Criteria," RSO Publication U-4972, Nov. 1971, Philco-Ford Corp., Newport Beach, Calif.

[24] Conard, P., Donaldson, DuP., and Snedeker, R., "A Study of the Modal Response Approach to Patterned Ablation Including Experiment Definition," SAMSO TN-70-213, April 1970, U.S. Air Force.

[25] Nachtsheim, P. R., "Stability of Cross-hatched Wave Patterns in Thin Liquid Films Adjacent to Supersonic Streams," *The Physics of Fluids*, Vol. 13, No. 10, Oct. 1970, pp. 2432–2447.

[26] Lane, F., "Viscoelastic-Material Version of the Self-Excitation Analysis for Striations of Ablating or Deforming Materials in Supersonic Flows with Turbulent Boundary Layers," KLD Technical Rept. 1, July 1971, KLD Associates, Huntington, N.Y.

[27] Grabow, R. M. and White, C. O., "A Surface Flow Approach for Predicting Cross-hatched Pattern Characteristics," *AIAA Journal*, Vol. 11, No. 6, June 1973, pp. 841–847.